REPORT DOCUMENTATION PAGE

Form Approved
OMB No. 0704-0188

1. REPORT DATE *(DD-MM-YYYY)*	**2. REPORT TYPE**	**3. DATES COVERED** *(From - To)*
09-05-2008	Technical Paper	

4. TITLE AND SUBTITLE

An Efficient Method for Calculating Surface Temperature and Heat Flux Based on Embedded Temperature Sensors (Preprint)

5a. CONTRACT NUMBER

5b. GRANT NUMBER

5c. PROGRAM ELEMENT NUMBER

6. AUTHOR(S)
Edward B. Coy (AFRL/RZSA)

5d. PROJECT NUMBER

5e. TASK NUMBER
50260548

5f. WORK UNIT NUMBER

7. PERFORMING ORGANIZATION NAME(S) AND ADDRESS(ES)

Air Force Research Laboratory (AFMC)
AFRL/RZSA
10 E. Saturn Blvd.
Edwards AFB CA 93524-7680

8. PERFORMING ORGANIZATION REPORT NUMBER

AFRL-RZ-ED-TP-2008-155

9. SPONSORING / MONITORING AGENCY NAME(S) AND ADDRESS(ES)

Air Force Research Laboratory (AFMC)
AFRL/RZS
5 Pollux Drive
Edwards AFB CA 93524-7048

10. SPONSOR/MONITOR'S ACRONYM(S)

11. SPONSOR/MONITOR'S NUMBER(S)
AFRL-RZ-ED-TP-2008-155

12. DISTRIBUTION / AVAILABILITY STATEMENT

Approved for public release; distribution unlimited (PA #08192A).

13. SUPPLEMENTARY NOTES

Submitted for presentation at the 26th AIAA Aerodynamic Measurement Technology Conference, to be held in Seattle, WA, 23-26 June 2008.

14. ABSTRACT

Approximate analytical solutions have been obtained for surface temperature and heat flux for the case of two embedded temperature sensors. The solutions have been verified and the range of validity has been established using several methods including comparisons with an exact analytical solution for a linear problem and numerical calculations for a non-linear problem. The performance of the model is presented in both the frequency domain and the time domain. A propagation of error analysis is presented and is used to establish the optimum spacing between the sensors. The solutions place no restrictions on the boundary or initial conditions and rely only on current values of temperature and its rate of change. The temperature dependence of transport properties is accounted for in an approximate way. The method requires minimal computation and is suitable for implementation as a real-time sensor.

15. SUBJECT TERMS

16. SECURITY CLASSIFICATION OF:			**17. LIMITATION OF ABSTRACT**	**18. NUMBER OF PAGES**	**19a. NAME OF RESPONSIBLE PERSON**
					Dr. Edward B. Coy
a. REPORT	**b. ABSTRACT**	**c. THIS PAGE**	SAR	11	**19b. TELEPHONE NUMBER** *(include area code)*
Unclassified	**Unclassified**	**Unclassified**			N/A

Standard Form 298 (Rev. 8-98)
Prescribed by ANSI Std. 239.18

An Efficient Method for Calculating Surface Temperature and Heat Flux Based on Embedded Temperature Sensors (Preprint)

Edward B. Coy[1]
Air Force Research Laboratory, Edwards AFB, CA, 93524

Approximate analytical solutions have been obtained for surface temperature and heat flux for the case of two embedded temperature sensors. The solutions have been verified and the range of validity has been established using several methods including comparisons with an exact analytical solution for a linear problem and numerical calculations for a non-linear problem. The performance of the model is presented in both the frequency domain and the time domain. A propagation of error analysis is presented and is used to establish the optimum spacing between the sensors. The solutions place no restrictions on the boundary or initial conditions and rely only on current values of temperature and its rate of change. The temperature dependence of transport properties is accounted for in an approximate way. The method requires minimal computation and is suitable for implementation as a real-time sensor.

Nomenclature

Fo	=	Fourier number, $\alpha t / x^2$
k	=	Thermal conductivity
T_i	=	Temperature
$\dot{T}_i$	=	Rate of change of temperature
t	=	Time
q	=	Heat Flux
x_i	=	Distance from heat flux surface
α_i	=	Thermal diffusivity
φ	=	Phase Angle
ω	=	Angular frequency

I. Introduction

THe measurement of transient heat flux and surface temperature in heat-sink combustion chambers continues to present technical challenges to the instrumentation engineer. Sensor failure rates are high and measurement accuracies and uncertainties are not well characterized. These shortcomings have had a significant impact on some recent programs which have used heat sink test articles to acquire data for the validation of heat transfer predictions at liquid rocket engine operating conditions[1,2].

There are numerous types of heat flux sensors but a relatively small subset is capable of operating in rocket chamber conditions where heat flux levels can exceed 10^8 W/m^2 and surface temperatures of 1000 K are typical. Diller[3] reviewed the devices that have been used and organized them into methods that rely on temperature differences over a spatial distance with known thermal resistance and temperature differences over time with known thermal capacitance. The most commonly used method has been the coaxial thermocouple which is an example of the second type. A thermocouple junction is formed on the surface of the chamber between a wire of one type of thermocouple material and a surrounding sheath of another type. The heat flux is determined from the measured temperature boundary condition using a one-dimensional transient solution to the heat equation. The junction is typically very thin and is often formed by lightly scratching the surface to drag filaments of one type of material

[1] Propulsion Research Engineer, Aerophysics Branch, Space and Missiles Propulsion Division, Propulsion Directorate, 10 East Saturn Blvd.

across the electrically insulating layer to the other type. In some applications, when erosion of the surface occurs the junction is continuously reformed and this has led to the description of coaxial thermocouples as "eroding thermocouples." However, in heat-sink chambers it is quite common to find that the junction disappears at some point during a test and the sensor fails.

Other methods have been developed which do not rely on surface temperature measurements but embed the sensors within the wall where they are protected from erosion. In the null-point calorimeter a hole is drilled from the backside of the chamber wall and a thermocouple is inserted. The bead is brazed or resistance welded to the bottom of the hole. "Null-point" refers to a distance from the bottom of the hole to the inner wall where the disturbance to the flow of heat caused by the hole results in the junction reading nearly equal to the inner wall temperature. The construction of null-point calorimeters is challenging. The junction cannot be visually inspected and large measurement errors can result from manufacturing flaws[4].

Another method using embedded temperature sensors is the plug-type heat flux gauge of Liebert[5]. An annular groove is machined into the chamber wall to form a post and thermocouples are attached at several axial points along the outside of the post. A polynomial curve is used to extrapolate the temperatures to the wall position and an integral method is used to calculate the total heat load to the plug from transient temperature measurements. Two-dimensional effects can be significant in this type of device. The dimensions of the groove are critical and significant errors can result from the disturbance to the flow of heat[6].

II. Derivation of Model

In the following analysis we adopt the approach of Liebert[5] of extrapolating a polynomial to the surface. The temperature profile in the body (see figure 1.) is approximated using a power series in x with time dependent coefficients.

$$T(x,t) = \sum_{i=0}^{n} c_i(t)\, x^n \tag{1}$$

However, in addition to matching the temperatures at the measurement points, the polynomial is also required to match the second derivatives with respect to x. These values are obtained from the time derivatives of temperature, which are assumed to be available as experimental measurements, and the heat equation.

$$\frac{\partial T}{\partial t} = \alpha \frac{\partial^2 T}{\partial x^2} \tag{2}$$

Adding these additional constraints allows a higher order polynomial to be used and markedly improves the time response of the sensor. Explicit expressions for the $c_i(t)$ can be obtained by substituting (1) into the right side of (2) then solving for the $c_i(t)$ in terms of the measured temperatures and their rates of change. For two measurement points there will be four measured quantities and the power series can be carried to the fourth term. If second derivatives are available, the series can be carried to the sixth term and so on.

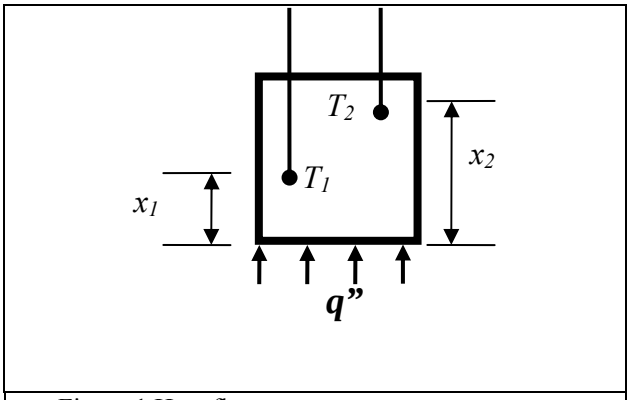

Figure 1 Heat flux sensor geometry

Evaluating the series at the surface, $x=0$, and combining terms in order to make the linear dependence on the measurements apparent, the temperature and heat flux expressions can be written as follows,

$$T_0 = T_1 \frac{x_2}{x_2 - x_1} + T_2 \frac{x_1}{x_2 - x_1} + \dot{T}_1 \frac{x_1 x_2 (2x_2 - x_1)}{6\alpha_1 (x_2 - x_1)} + \dot{T}_2 \frac{x_1 x_2 (x_2 - 2x_1)}{6\alpha_2 (x_2 - x_1)} \tag{3}$$

$$q_0 = -k(T_0)\left(T_1 \frac{-1}{x_2 - x_1} + T_2 \frac{1}{x_2 - x_1} + \dot{T}_1 \frac{x_1^2 - 2x_1 x_2 - 2x_2^2}{6\alpha_1 (x_2 - x_1)} + \dot{T}_2 \frac{2x_1^2 + 2x_1 x_2 - x_2^2}{6\alpha_2 (x_2 - x_1)} \right) \tag{4}$$

In deriving these solutions, no assumptions have been made with respect to the boundary conditions at the top of the block and in fact it is completely arbitrary. For example, the top surface could be actively cooled. Also the second sensor at x_2 does not need to be embedded within the block and can be located at the top surface. The sensor at x_1 may be located at the $x=0$ surface. Furthermore, we have made no assumptions with respect to the origin of time. The solution relies only on the current values of temperature and rates of change of temperature. Referring back to the categorizations of methods defined by Diller[3], this method is a hybrid of the two types as it relies on both spatial and temporal variations in temperature.

The method used to evaluate the rate of change of temperature is critical to the success of the technique. A simple finite difference calculation will almost certainly result in an unacceptable level of noise in the derivative. A polynomial smoothing filter, also known as a Savitzky-Golay[7,8] filter, can be effective in reducing noise and can be calculated very efficiently. The filter is implemented as a convolution in the time domain.

$$T(t_n) = \sum_{i=-m}^{m} a_i T(t_{n+i}) \tag{5}$$

$$\dot{T}(t_n) = \sum_{i=-m}^{m} b_i T(t_{n+i}) \tag{6}$$

Substituting (5) and (6) into (3) and (4) we arrive at the final forms for the surface temperature and heat flux expressions.

$$T_0(t_n) = \sum_{i=-m}^{m} e_i T_1(t_{n+i}) + f_i T_2(t_{n+i}) \tag{7}$$

$$q_0(t_n) = -k(T_0) \sum_{i=-m}^{m} g_i T_1(t_{n+i}) + h_i T_2(t_{n+i}) \tag{8}$$

The coefficients are defined as follows.

$$e_i = a_i \frac{x_2}{x_2 - x_1} + b_i \frac{x_1 x_2 (2x_2 - x_1)}{6\alpha_1 (x_2 - x_1)} \tag{9}$$

$$f_i = a_i \frac{x_1}{x_2 - x_1} + b_i \frac{x_1 x_2 (x_2 - 2x_1)}{6\alpha_2 (x_2 - x_1)} \tag{10}$$

$$g_i = a_i \frac{-1}{x_2 - x_1} + b_i \frac{x_1^2 - 2x_1 x_2 - 2x_2^2}{6\alpha_1 (x_2 - x_1)} \tag{11}$$

$$h_i = a_i \frac{1}{x_2 - x_1} + b_i \frac{2x_1^2 + 2x_1x_2 - x_2^2}{6\alpha_2 (x_2 - x_1)} \tag{12}$$

Note that once the coefficients have been calculated, only 4m+2 multiplications and 2m+1 additions are required to evaluate T_0 and q_0, or about 100 processor operations are required for a typical value for m of 10.

The uncertainties δT_0 and δq_0 can be evaluated by treating each temperature measurement as an independent random variable and using the "square root of the sum of squares" approach. We also assume that uncertainties in thermocouple locations and material properties are negligible.

$$\delta T_0(t_n) = \left(\sum_{i=-m}^{m} e_i^2 \, \delta T_1^2 + f_i^2 \delta T_2^2 \right)^{1/2} \tag{13}$$

$$\delta q_0(t_n) = k(T_0) \left(\sum_{i=-m}^{m} g_i^2 \, \delta T_1^2 + h_i^2 \delta T_2^2 \right)^{1/2} \tag{14}$$

Minimum values of δT_0 and δq_0 can be achieved by making an optimum choice for the order of the polynomial used to obtain the a_i and b_i. For a fixed level of uncertainty in the measurements, the coefficients of a high order method will result in a larger value for the total uncertainty; however, in the presence of high frequency content, a high order polynomial will fit the trend more closely and reduce the values of δT_n, thereby reducing the total uncertainty. The optimum order can be found by increasing the order until a minimum in the uncertainty is found. However this increases the amount of computation and in practice we find that the quadratic smoothing filter is a good compromise and can be used as the default method. The coefficients for the quadratic smoothing filter are the following.

$$a_i = \frac{\dfrac{1}{\sum_{j=-m}^{m} j^2} - \dfrac{i^2}{\sum_{j=-m}^{m} j^4}}{\dfrac{2m+1}{\sum_{j=-m}^{m} j^2} - \dfrac{\sum_{j=-m}^{m} j^2}{\sum_{j=-m}^{m} j^4}} \tag{15}$$

$$b_i = \frac{i}{\Delta t \sum_{j=-m}^{m} j^2} \tag{16}$$

III. Verification of Model

To illustrate the behavior of the approximate solutions, we make comparisons with the exact solution for the temperature within a semi-infinite slab exposed to an oscillating heat flux at the surface.

$$q_0 = \bar{q} \cos(\omega t) \tag{17}$$

$$T(x,t) = T_0 + \frac{\bar{q}}{k} \left(\frac{\alpha}{\omega} \right)^{1/2} \exp\left(-x \left(\frac{\omega}{2\alpha} \right)^{1/2} \right) \cos\left(\omega t - x \left(\frac{\omega}{2\alpha} \right)^{1/2} - \frac{\pi}{4} \right) \tag{18}$$

When (18) and its time derivative are substituted into (3) and (4) the results are linear combinations of sine and cosine terms of the form:

$$T_0 = A\cos(\omega t + \phi_1) + B\cos(\omega t + \phi_2) + C\sin(\omega t + \phi_1) + D\sin(\omega t + \phi_2) \tag{19}$$

The four terms can be combined into a single term of the following form.

$$T_0 = Gain\,\frac{\overline{q}_0}{k}\left(\frac{\alpha}{\omega}\right)^{1/2}\sin(\omega t + Phase) \tag{20}$$

The amplitude and phase behaviors are shown in figures 2 and 3. For greater generality, the results are plotted as functions of two non-dimensional numbers. The x-axis is a non-dimensional angular frequency which is the reciprocal of a Fourier number based on the angular frequency of the heat flux and the distance from the surface to the first sensor, $Fo^{-1} = x_1^2\omega/\alpha$, and the individual curves are for various values of the ratio x_2/x_1. These two variables completely determine the solutions. Considering the surface temperature first, we see immediately that the solution has the characteristics of a low pass filter but with a region of positive gain in the range of angular frequencies from 1 to 20. We also see that the magnitude of the gain increases with the ratio x_2/x_1. The phase of the solution begins to lag at angular frequencies above 1 except for x_2/x_1=4 where there is a range from 0.4-4 where the phase angle is positive.

The behavior of the solution for heat flux is given in figure 3 and is substantially similar. In this case, the peak in the gain increases with x_2/x_1 but is significantly lower than the peak in the surface temperature gain. In fact, for heat flux, the gain behavior is quite a weak function of x_2/x_1 over the range from 1.5-4. The phase behavior is also a weak function of x_2/x_1 with all values showing a roll off beginning near an angular frequency of 0.5.

In addition to correctly reproducing the amplitude and phase of a heat flux signal, the model must also be robust in the presence of noise. We now consider the effect of the parameter x_2/x_1 on the propagation of error from noise in the temperature measurements. Equations (13) and (14) are expressions for the uncertainties in surface temperature and heat flux when the smoothing filter approach has been used. An alternative approach for deriving these expressions is to start with (3) and (4) and assume that the uncertainties in temperature and rate of change of temperature are known quantities. This approach yields succinct expressions that reveal the role of x_2/x_1. We assume the error in each measurement is independent and the thermocouple positions and material properties are error free. The sensitivity coefficients are simply the coefficients in (3) and (4). If we assume $\delta T_1 \approx \delta T_2$, $\delta\dot{T}_1 \approx \delta\dot{T}_2$ and $\alpha_1 \approx \alpha_2$, the uncertainty of the surface temperature is,

$$\delta T_0 = \sqrt{\frac{x_2^2 - x_1^2}{(x_2 - x_1)^2}\delta T^2 + \frac{x_1^2 x_2^2 (5x_2^2 - 8x_1x_2 + 5x_1^2)}{36\alpha^2 (x_2 - x_1)^2}\delta\dot{T}^2} \tag{21}$$

The uncertainty for the heat flux is,

$$\delta q_0 = k(T_0)\sqrt{\frac{1}{(x_2 - x_1)^2}\delta T^2 + \frac{(5x_1^4 + 4x_1^3x_2 + 4x_1x_2^3 + 5x_2^4)}{36\alpha^2 (x_2 - x_1)^2}\delta\dot{T}^2} \tag{22}$$

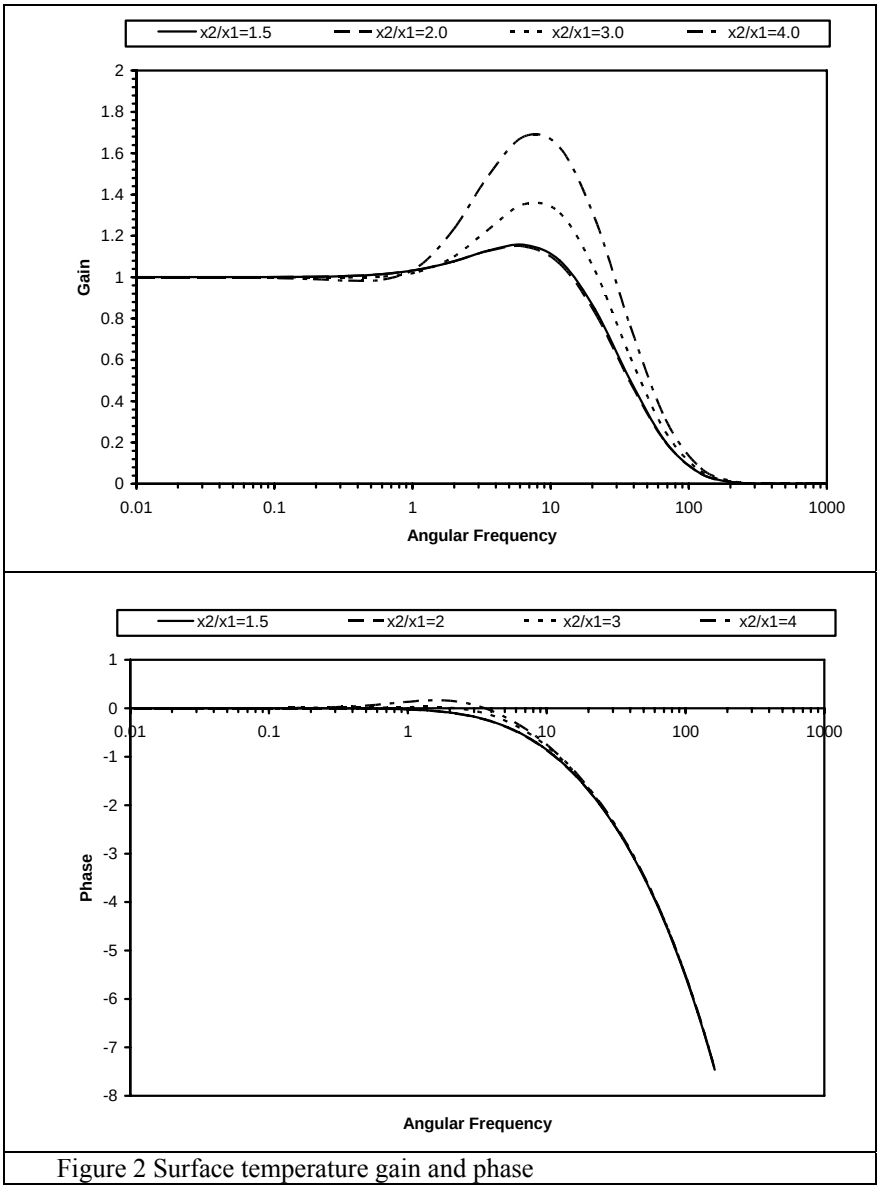

Figure 2 Surface temperature gain and phase

Equations (21) and (22) show that uncertainty is a function of the positions of the sensors, and therefore we can anticipate that there will be optimum locations that minimize uncertainty. To make quantitative predictions we need estimates for δT and $\delta \dot{T}$ and these were obtained from experimental data that will be presented later. The specific values used here were δT =1 K and $\delta \dot{T}$ = 20 K/s. Figure 4 shows the uncertainty in surface temperature based on (21) and in fact it has a minimum at x_2/x_1=3.6, but the minimum is quite broad and any value from 2.3 to 5 would work as well. This region corresponds well to the region of maximum accuracy identified previously. However, the uncertainty increases rapidly for x_2/x_1<2 so this range should be avoided. The minimum in the heat flux uncertainty (Figure 5) based on (22) is somewhat sharper with the optimum value 2.3. The heat flux uncertainty has been normalized by the magnitude of the heat flux so it can be seen that the minimum in the uncertainty is approximately 0.75% of the measured value. Again, values of x_2/x_1<2 should be avoided. Based on these uncertainty estimates plus the gain and phase results described above, the optimum value for x_2/x_1 is 2.3-2.5.

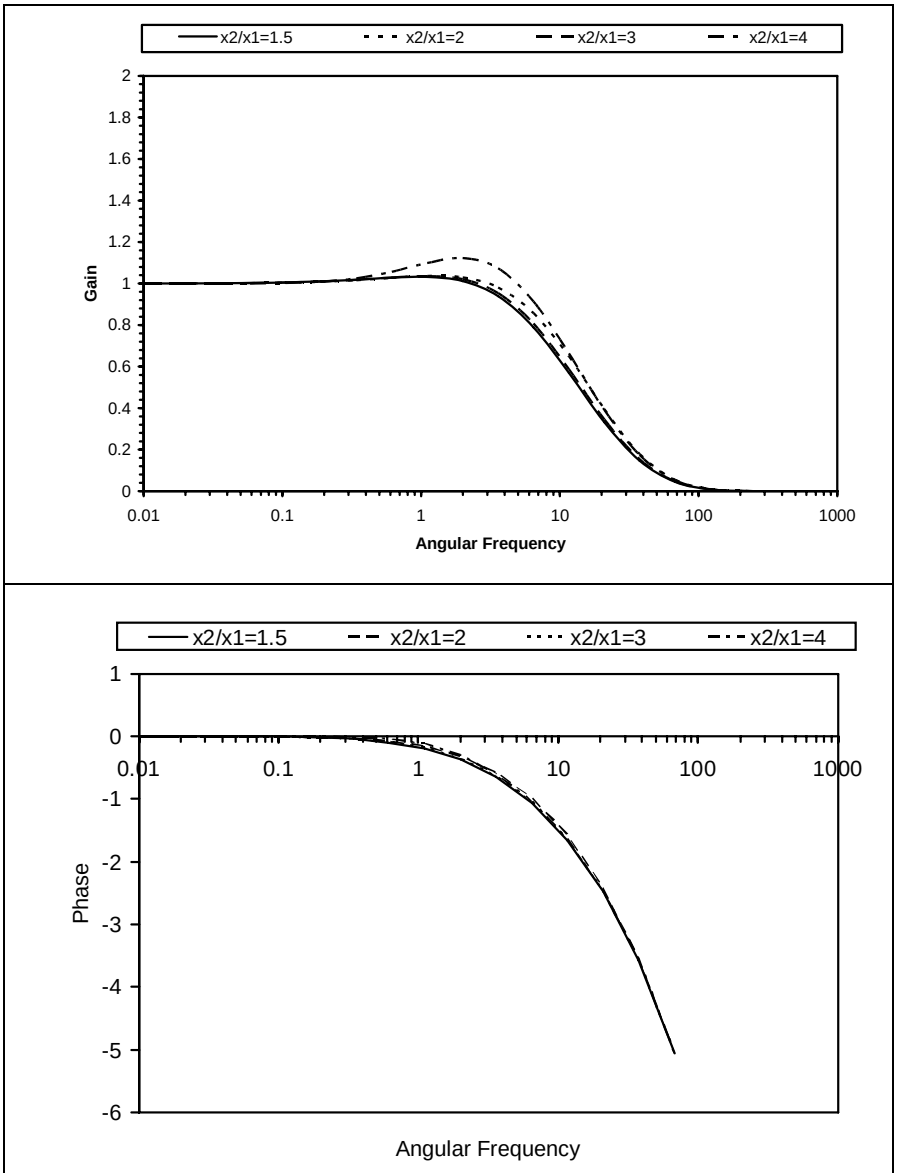

Figure 3 Heat flux gain and phase

IV. Temperature Dependent Properties

If thermal properties are temperature dependent the heat equation is non-linear and analytical solutions such as (18) are not possible. For this case the model was verified and validated using numerical results. We chose as a test case an idealized version of the typical test conditions we see in our laboratory: a step change in heat flux from 0-$4x10^7$ W/m^2. The MatLab non-linear PDE solver, pdepe was used to generate temperature histories for the surface and internal points and these were converted back to heat flux and surface temperature using the model. Two cases of x_2/x_1 are shown. For both cases the sensor nearest the surface is located at a depth of 1.905 mm (0.075 inch). The total thickness of the slab was 41.91 mm (1.65 inch) and the material was high-conductivity copper. The heat flow was assumed to be one-dimensional. The grid contained 131 evenly spaced points and the temperatures were saved at one millisecond intervals. Results using a 261 point grid differed by approximately 0.1 K and did not change the model results.

The ability of the model to reproduce the surface temperature and heat flux boundary conditions is shown in figure 6. For both cases of x_2/x_1, after 0.1 seconds the polynomial model has converged to within 0.1 K for the surface temperature and within 1% of the heat flux, but the magnitude of the overshoot is significantly smaller for x_2/x_1=2.3 than 3 as we should expect from the gain plots presented earlier.

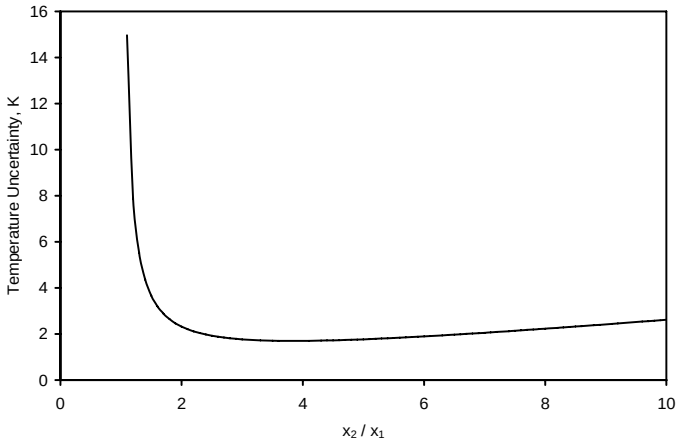

Figure 4 Temperature Uncertainty

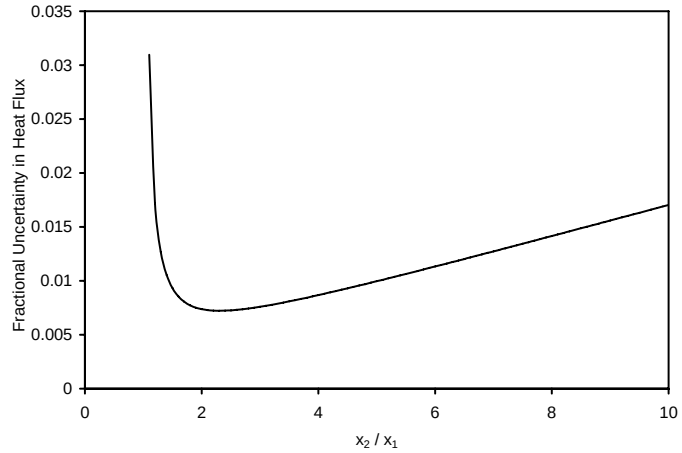

Figure 5 Heat Flux Uncertainty

V. An Application of the Model

To illustrate the application of the model we present data taken in a sub-scale, heat-sink, rocket combustion chamber. Type K thermocouples were embedded in a high conductivity copper block that formed one side of a 2.54 cm square channel. The locations of the sensors were those given above in the description of the temperature-dependent properties calculation. The reactants were gaseous hydrogen and gaseous oxygen at a mass flow rate ratio of 1:5.5. The propellants were completely mixed and reacted at the measurement location. The pressure of the chamber was 42 bar (600 psig) and the mean velocity of the gas was approximately 250 m/s (820 ft/s). In figure 7 the upper figure shows the temperatures measured within the block labeled as "Front Side" for x_1 and "Backside" for x_2. Also shown are results for surface temperature based on (3) and uncertainty based on (13) which is read on the right-side vertical axis. The reference in the legend to Tsurf3 and T3 refers to the data from the third of six measurement positions. In this example, which used an early version of the technique, the uncertainties of the temperatures and rates of change of temperature were obtained from the uncertainties in linear regression parameters over a data window 60 milliseconds wide and containing 61 measurements. This is equivalent to a polynomial smoothing filter based on a linear function in distinction to the quadratic filter recommended above and given in (15) and (16). The uncertainties increase in the regions where the rates of change of temperature are not constant as occurs at the beginning and end of the test and are largely due to the fact that the linear regression was used. The uncertainties propagate to the surface temperature calculation resulting in the spikes at 1.6 and 2.2 seconds. The heat flux results are shown in the lower figure. The maximum value reached was 2.46×10^7 W/m^2 (15.0 Btu/in^2/s). The uncertainty in heat flux due to noise during the middle of the run is approximately 0.5% of the measured value.

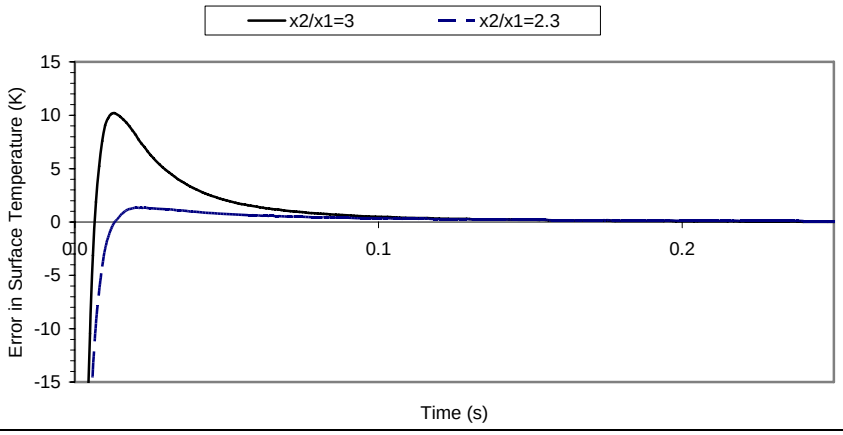

Figure 6a Effect of temperature dependent properties on surface temperature prediction. Test case is step change in heat flux from 0 to 4e7 W/m2 (24.5 Btu/in2/s).

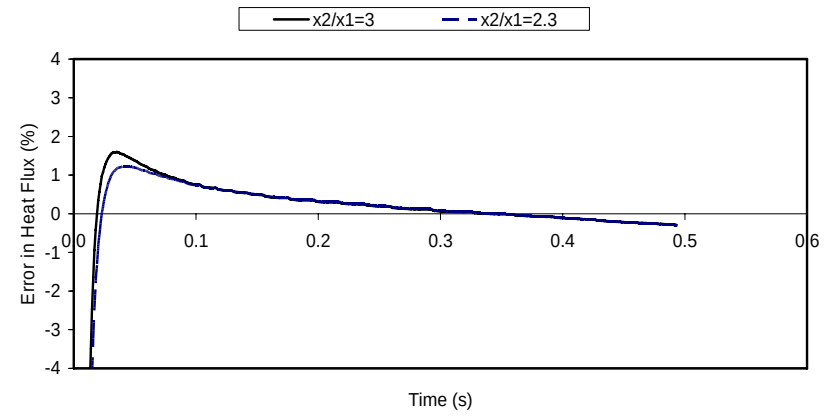

Figure 6b Effect of temperature dependent properties on accuracy of heat flux. Test case is a step change in heat flux from 0-4e7 W/m^2 (24.5 Btu/in^2/s). Heat flux converges to within 1% after 0.1 seconds.

VI. Conclusion

A method has been described for measuring surface temperature and heat flux based on two temperature sensors embedded in the wall of a chamber. The method does not require surface junction thermocouples which are prone to failure and produce noisy signals in rocket engine flows and is well suited for studies of the effects of surface features on heat transfer enhancement. A polynomial extrapolation approach is used where the function is constrained to match the temperatures and the second derivatives with respect to distance at the measurement points. The method requires only current values of temperature and its rate of change and the boundary and initial conditions are arbitrary. The algorithm can be represented as a low pass filter and the gain and phase behavior have been characterized. The placement of the sensors affects the frequency cutoff and the noise response and optimum values for the relative positions of the sensors have been obtained. The method utilizes time derivatives of temperature data which can be efficiently calculated using a polynomial smoothing filter. The method is computationally efficient, requiring approximately 100 multiply and add operations and is suitable for implementation in a digital signal processor.

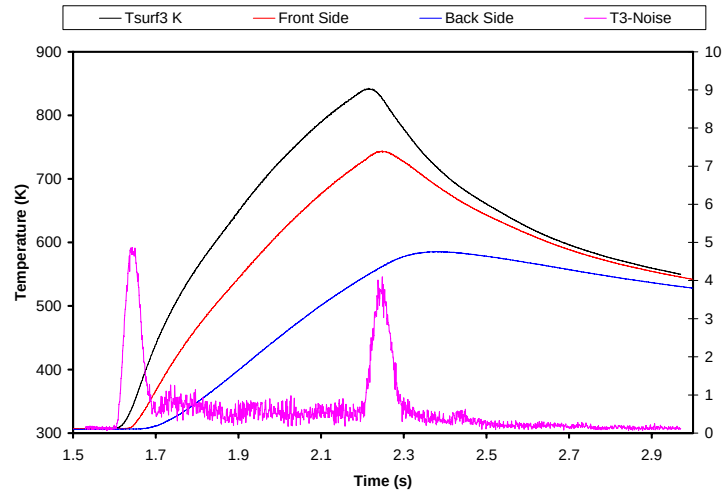

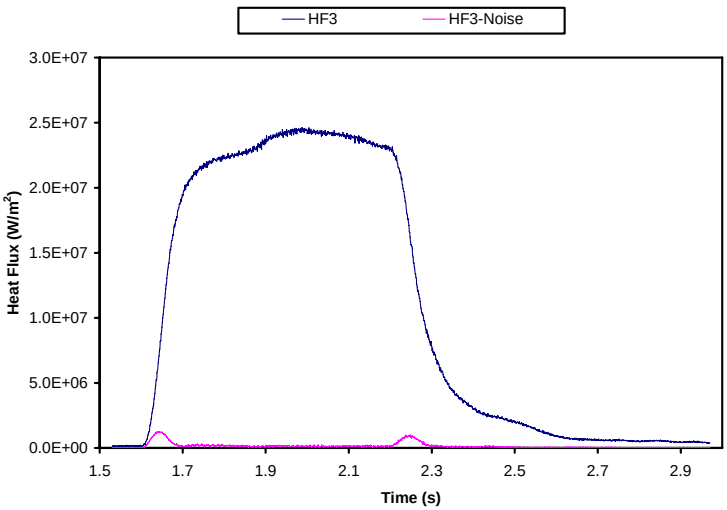

Figure 7 Surface temperature and heat flux from experimental data obtained in a subscale rocket combustion chamber

References

[1] Droppers, L.J., Schuff, R., Anderson, W., "Study of Heat Transfer in a Gaseous Hydrogen Liquid Oxygen Multi-Element Combustor, AIAA 2007-5550

[2] Jones, G,. Protz, C., Bullard, B., Hulka, J., "Local Heat Flux Measurements with Single Element Coaxial Injectors," AIAA 2006-5194

[3] Diller, T.E., "Advances in Heat Flux Measurement," in Advances in Heat Transfer, Vol. 23, pp. 279-368, 1993

[4] Kidd, C.T., "Recent developments in high heat-flux measurement techniques at the AEDC," Proceedings of 36th International Instrumentation Symposium, ISA, Research Triangle Park, NC, pp. 35-44

[5] Liebert, C.H., "Measurement of local high-level, transient surface heat flux," NASA TP-2840, 1988

[6] Rooke, S., Fralick, G., Liebert, C., "Heat Transfer Analysis of a Plug-Type Heat Flux Gauge," J. of Thermophysics and Heat Transfer, Vol. 12, No. 4, October-December, 1998, pp. 536-542

[7] Press, W.H., Teukolsky, S.A., Vetterling, W.T., Flannery, B.P., Numerical Recipes in Fortran, 2nd ed., Cambridge University Press, 1993

[8] Savitzky, A., Golay, M., "Smoothing and Differentiation of Data by Simplified Least Squares Procedures," Analytical Chemistry, Vol. 36, No. 8, pp. 1627-1639, 1964